The effects of proton tunneling, 14N quadrupole coupling, and methyl internal rotations in the microwave spectrum of ethyl methyl amine

Kenneth J Koziol, Wolfgang Stahl, Ha Vinh Lam Nguyen

The Journal of Chemical Physics

The Effects of Proton Tunneling, ^{14}N Quadrupole Coupling, and Methyl Internal Rotations in the Microwave Spectrum of Ethyl Methyl Amine

Kenneth Jan Koziol,[a] Wolfgang Stahl,[a] and Ha Vinh Lam Nguyen[b,c*]

[a] *Institute of Physical Chemistry, RWTH Aachen University, Landoltweg 2, 52074 Aachen, Germany.*

[b] *Laboratoire Interuniversitaire des Systèmes Atmosphériques (LISA), CNRS UMR 7583, Université Paris-Est Créteil, Université de Paris, Institut Pierre Simon Laplace, 61 avenue du Général de Gaulle, 94010 Créteil, France.*

[c] *Institut Universitaire de France (IUF), 1 rue Descartes, 75231 Paris cedex 05, France.*

* Corresponding author. Email: lam.nguyen@lisa.u-pec.fr

The spectra of *N*-ethyl methyl amine, $CH_3(NH)CH_2CH_3$, were measured using a molecular jet Fourier transform microwave spectrometer in the frequency range of 2 to 26.5 GHz. Splittings due to proton inversion tunneling, Coriolis coupling, ^{14}N quadrupole coupling, and methyl internal rotation were fully resolved. The experimentally deduced rotational constants are A = 25934.717(21) MHz, B = 3919.8212(23) MHz, and C = 3669.530(21) MHz. The proton tunneling causes (+) ↔ (−)splittings of about 1980.9 MHz for all *c*-type transitions between the lowest symmetric and the higher anti-symmetric energy levels. The splittings influenced by Coriolis coupling for *b*-type transitions were also observed and assigned, yielding the coupling constants F_{bc} = 0.3409(71) MHz and F_{ac} = 163.9(14) MHz. The ^{14}N quadrupole coupling constants were determined to be χ_{aa} = 2.78865(55) MHz and $\chi_{bb} - \chi_{cc}$ = 4.45665(91) MHz. Fine splittings arising from two inequivalent methyl rotors are in the order of 150 kHz, and the torsional barriers are determined to be 1084.62(41) cm^{-1} for the **CH$_3$**NH methyl group and 1163.43(80) cm^{-1} for the CH$_2$**CH$_3$** methyl group. The experimental results are in good agreement with those of quantum chemical calculations.

I. INTRODUCTION

Microwave spectroscopy is an established analytical method to retrieve information about the gas-phase conformational structures of small to medium-sized organic molecules with the only requirement that the molecules of interest have a permanent dipole moment. The rotational spectra are conformational specific and allow the detection and characterization of each individual conformer of the molecules.

Two major fields of research that employ microwave spectroscopy are atmospheric chemistry and astrophysics. The development of models for atmospheric chemistry are of fundamental importance to understand the concepts of climate and processes in our atmosphere[1] with extensive researches about chemical compositions and direct changes on the radiative forcing of the atmosphere.[2] Within the lower troposphere, the spectra of smaller organic molecules lead to key information about the origin of such compounds, as demonstrated in the works of Blumestock et. al. with the detection of unusual chlorine activation during the arctic winter.[3] This atmospheric research has been extended to other planets and within our solar system. Muhleman and Clary have reported the rotational spectra of H_2O, CO, O_2, O_3, and H_2O_2 in the atmosphere of Mars, which helped for a better understanding of the water cycle and composition of the Mars atmosphere.[4] Many organic compounds have been also identified in the interstellar medium (ISM) by rotational spectroscopy, for example the detection of methyl acetate and *gauche* ethyl formate in the Orion Nebula,[5] followed by the detection of ethyl formate in the giant molecular cloud Sagittarius B2 near the center of the Milky Way Galaxy. A complete list of all molecules previously detected in the ISM can be found i.a. at the Cologne Database for Molecular Spectroscopy (CDMS) website.[6] Among around 200 molecules detected in the ISM or circumstellar shells,[6] none of them are secondary amines, despite the importance of this class of compound in biology and chemistry. This is most probably because of the lack of an important step towards the detections of new molecules in the ISM, which is the laboratory investigation of rotational spectra of those molecules, as pointed out in a recent review by Kleiner.[7] So far, the spectra of only three linear aliphatic secondary amines have been studied by high resolution microwave spectroscopy, which are dimethyl amine[8], ethyl methyl amine (EMA),[9] and diethyl amine.[10]

This class of molecules is particularly interesting for spectroscopic researches, featuring a multitude of different effects that can occur in the microwave spectra. The terminal methyl groups undergo internal rotations that cause fine splittings into different species. The magnitude of these splittings depends on the torsional barrier height. The ^{14}N nucleus causes a quadrupole hyperfine structure in the margin of few hundreds of kHz to several MHz. Finally, an effect of great interest in the cases of planar secondary amines is the proton tunneling. The tunneling motion of the proton attached to the nitrogen atom causes the *c*-dipole moment component to change its sign, resulting in splittings of the otherwise degenerate (+) and (−) species of all rotational levels. Such tunneling

splittings of 2646.0 MHz, 1981.0 MHz, and 1521.5 MHz have been reported for dimethyl amine,[8] EMA,[9] and diethyl amine,[10] respectively.

While the microwave spectrum of diethyl amine has been measured and analyzed to great accuracy,[10] previous studies on dimethyl amine by Wollrab and Laurie[8] as well as on EMA by Penn and Boggs,[9] both utilizing Stark modulated microwave spectrometers, only focused on the proton tunneling. The effects of ^{14}N quadrupole coupling and methyl internal rotation were not taken into account because the splittings were below the resolution limit. In the present work, we apply the state-of-the-art molecular jet Fourier transform microwave spectroscopy (MJ-FTMW) technique with much higher resolution in combination with modern quantum chemical calculations to revisit the spectrum of EMA. The microwave spectrum of dimethyl amine is the subject of an on-going reinvestigation.

II. THEORETICAL SECTION

A. Quantum Chemical Calculations

All quantum chemical calculations for EMA were carried out using the *Gaussian 09* package.[11] The molecule possesses two inequivalent methyl internal rotors and a ^{14}N nucleus. The optimizations were performed on a series of 12 starting geometries where the hydrogen atom of the amino group was set to be out of plane by an angle $\beta = \angle(H_2,C_3,N_1,C_7)$ of 60° and the dihedral angle $\theta = \angle(C_3,N_1,C_7,C_{10})$, corresponding to a rotation of the ethyl group about the N_1-C_7 bond, was altered in steps of 30° (for atom numbering, see Figure 1). All bond lengths and bond angles were allowed to relax during the optimizations. Three methods that were employed are the Møller-Plesset perturbation theory (MP2) and the density functional theory (DFT) with the Becke, three-parameter, Lee-Yang-Parr (B3LYP) and the Becke, three-parameter, Perdew-Wang (B3PW91) functionals, in combination with the Pople-zeta basis set 6-311++G(d,p). Three stable conformers were obtained, where in conformer I, all heavy atoms are located in one plane while in conformers II and III, the methyl group tilts out of the C-N-C plane by about 60° as shown in the Newman projection in Figure 2. The geometry of conformer I from MP2 optimizations is illustrated in Figure 1, showing the two energetically equivalent structures and the *c*-dipole moment component.

The nuclear coordinates of all three conformers calculated at MP2, B3LYP, and B3PW91 levels of theory are presented in Table S-I in the Supporting Information. Potential energy curves were also calculated by varying the angle θ in steps of 10°, while all other geometry parameters were allowed to relax. The data were fitted using a Fourier expansion given in Eq. S-I in the Supporting Information. The respective symmetry-adapted Fourier

coefficients are available in Table S-II. The potential curves were drawn as contour plots using these coefficients and presented Figure 2.

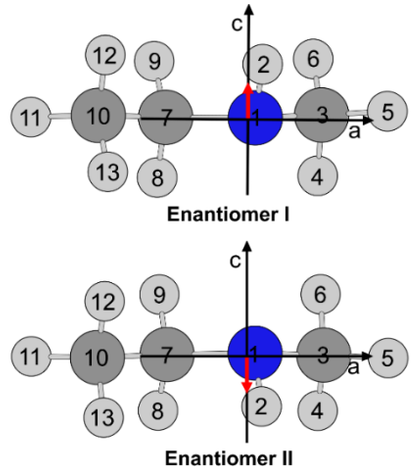

FIG. 1: Two equilibrium geometries of the most stable conformer I of ethyl methyl amine in the principal axes of inertia calculated at the MP2 level of theory, corresponding to the two energy minima of the proton tunneling process. The red arrows represent the *c*-component of the dipole moment vector, which changes sign upon proton tunneling.

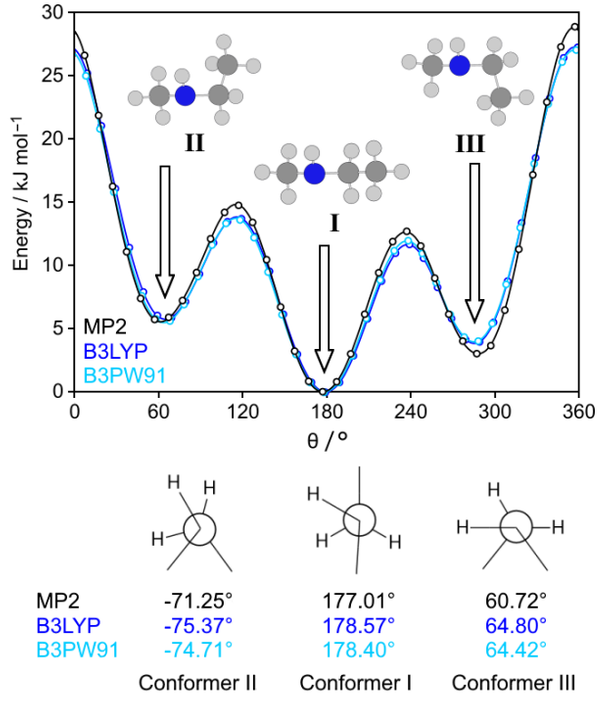

FIG. 2: Upper figure: Potential energy curves of EMA by varying the dihedral angle $\theta = \angle(C_3,N_1,C_7,C_{10})$ in steps of 10° while all other geometry parameters were optimized at the MP2/6-311++G(d,p) (black), B3LYP/6-311++G(d,p) (blue), and B3PW91/6-311++G(d,p) (cyan) levels of theory. Energies are given relative to the absolute energy of –173.9775473, –174.5369953, and –174.469586 Hartree, respectively, of the minima. Lower figure: Newman projection along the C_3–N_1 bond. The angles θ are given for each conformer.

Aside from the relative energy between the different conformers, we also determined the barrier height for a conformational switch. The barrier height between conformers I and II, ΔE_{12}, is the lowest with a value of 977.67 cm^{-1} (11.7 $kJ{\cdot}mol^{-1}$), 1003.04 cm^{-1} (12.0 $kJ{\cdot}mol^{-1}$), and 1061.07 cm^{-1} (12.7 $kJ{\cdot}mol^{-1}$) predicted at the B3LYP, B3PW91, and MP2 levels of theory, respectively, while the barrier between conformer I and III, ΔE_{13}, is higher with a value of, e.g., 1233.27 cm^{-1} (14.8 $kJ{\cdot}mol^{-1}$) for MP2. The highest barrier is needed to switch conformers II and III (2415.58 cm^{-1}, i.e. 28.9 $kJ{\cdot}mol^{-1}$, from calculations at the MP2 level of theory). There is a trend that values calculated with the MP2 method are higher than those obtained with a DFT method. All results are given in Table S-III in the Supporting Information. As the relaxation barrier is quite high, conformational relaxation is thus unlikely. Due to the low rotational temperature under jet-cooled measurement conditions, we only expect the most stable conformer I to be present in our spectrum. Therefore, this conformer will be discussed in detail. Results of the calculations for conformers II and III are found in the Supporting Information.

For conformer I, the value of the *A* rotational constant predicted at the MP2/6-311++G(d,p) level of theory is 26059.1 MHz, by one order of magnitude larger than that of 3929.0 MHz and 3678.0 MHz for the *B* and the *C* constant, respectively. Conformer I of EMA is thus a near prolate top with a Ray's asymmetry parameter $\kappa = -0.978$.[12] The results of the quantum chemical calculations for the conformers of EMA are presented in Table I.

TABLE I: Optimized energy *E*, energy difference ΔE relative to that of conformer I, dihedral angle θ, rotational constants *A*, *B*, *C*, and Ray's parameters κ of EMA calculated at the MP2/6-311++G(d,p) level of theory.

Conf.	θ / °	*E* / Hartree	ΔE / $kJ{\cdot}mol^{-1}$	*A* / GHz	*B* / GHz	*C* / GHz	κ[a]
I	177.0	−173.977547	0.00	26060.1	3929.0	3678.0	–0.978
II	288.8	−173.976409	2.99	14534.8	5111.6	4340.0	–0.849
III	60.7	−173.975414	5.60	14320.7	5074.1	4330.20	–0.851

[a] Ray's parameter κ is defined as $\kappa = \frac{2B-A-C}{A-C}$.

The dipole moment components calculated with the MP2 method are $|\mu_a|$ = 0.05 D, $|\mu_b|$ = 0.39 D, and $|\mu_c|$ = 1.08 D. Unlike the cases of dimethyl amine and diethyl amine where the dipole moment component in the *a*-direction is zero due to symmetry,[8,10] the tiny but non-zero *a*-component of EMA suggests that the *a*-type spectrum is extremely low in intensity but existential. The *c*-type spectrum is expected to be very intense, and *b*-type transitions should be much weaker but measurable.

B. ^{14}N Nuclear Quadrupole Coupling Constants

The electric field gradients q_{ii} (i = a, b, c) in the principal axis system were calculated from the optimized structures at the MP2, B3LYP, and B3PW91 levels of theory, using the B3PW91 method and the basis set 6-311+G(df,pd). The quadrupole constants were corrected with a factor of eQ/h of 4.562 MHz where e is the elementary charge, Q is the electric quadrupole moment of the ^{14}N nucleus, and h is Planck's constant. The value of eQ/h is taken as a best-fit parameter determined by linear regression analysis of calculated q_{ij} on the experimental structures of a series of different nitrogen containing molecules versus the corresponding experimental χ_{ij}, a method introduced by Bailey.[13-15] The calculated quadrupole coupling constants and dipole moment components are assembled in Table II.

TABLE II: Dipole moment components alongside the axes of inertia μ_a, μ_b, μ_c and quadrupole constants χ_{aa}, χ_{bb}, χ_{cc} of EMA calculated at the MP2/6-311++G(d,p) level of theory.

Conf.	$\lvert\mu_a\rvert$ (D)	$\lvert\mu_b\rvert$ (D)	$\lvert\mu_c\rvert$ (D)	$\lvert\mu\rvert$ (D)	$\lvert\chi_{aa}\rvert$ (MHz)	$\lvert\chi_{bb}\rvert$ (MHz)	$\lvert\chi_{cc}\rvert$ (MHz)
I	0.051	0.392	1.075	1.146	2.7790	0.8388	3.6178
II	0.227	0.290	1.102	1.162	2.5126	2.3035	4.8161
III	0.606	0.913	0.477	1.195	1.0627	2.3690	1.3063

C. Internal Rotation

Ethyl methyl amine has two inequivalent methyl groups undergoing internal rotation. The **CH$_3$**NH– methyl rotor will be called henceforward the amino methyl group i_M and the –CH$_2$**CH$_3$** methyl rotor the ethyl methyl group i_E. The barriers to internal rotation of both methyl groups were also calculated with the MP2, B3LYP, and B3PW91 methods and the basis set 6-311++G(d,p). The dihedral angles α_1 = ∠(C_7,N_1,C_3,H_4) and α_2 = ∠(N_1,C_7,C_{10},H_{11}) defining the torsion of the internal rotation were altered in steps of 10° for 120°, while all other geometry parameters were optimized. The obtained energies were parameterized by a Fourier expansion with the symmetry adapted coefficients given in Table S-IV. The potential energy curves drawn as a contour plot from these coefficients are shown in Figure S-I to S-III in the Supplementary Material.

The energy points form typical three-fold potentials with barrier heights of 1105.10 and 1178.84 cm^{-1} for the amino and the ethyl methyl group, respectively, in calculations with the MP2 method. The respective values from calculations with the B3LYP functional are 1023.12 and 1070.44 cm^{-1}, as well as 1024.68 and 1081.40 cm^{-1} with the B3PW91 functional. Obviously, the torsional barriers of the ethyl methyl group are higher than that of the amino methyl group. Probably, the neighboring methylene group is responsible for the sterical hindrance and

a repulsive Coulomb force which increases the barrier to internal rotation of the ethyl methyl group, while the torsion of the amino methyl group is less hindered by the amino group. The barrier heights for conformers II and III are given in Table S-V in the Supplementary Material.

In the previous microwave study on diethyl amine, splittings arising from two equivalent ethyl methyl groups could be resolved, and a torsional barrier of 1051.74(57) cm^{-1} was deduced.[10] The two equivalent ethyl methyl groups in diethyl ketone and the ethyl methyl group in methyl propionate or in the two conformers of 2-propionylthiophene undergo internal rotation with barrier heights of 771.93(27) cm^{-1},[16] 820.46(99) cm^{-1},[17] 806.94(54) cm^{-1}, and 864.5(88) cm^{-1},[18] respectively, resulting also in resolvable splittings in the rotational spectrum. In a series of n-alkyl ketones, starting from propyl methyl ketone (pentan-2-one) to heptan-2-one, the terminal alkyl methyl group always shows resolvable splittings associating with a torsional barrier around 1000 cm^{-1}.[19-21] Therefore, we expect that splittings arising from internal rotation of the ethyl methyl group in ethyl methyl amine are also observable in the microwave spectrum, and probably also those from the amino methyl group.

D. Proton Inversion Tunneling

Results of the geometry optimizations reveal that all heavy atoms of the energetically most stable conformer I are located in the *ab*-plane. The amino hydrogen can on either side of this plane, resulting in two energetically equivalent structures which are enantiomers and have different signs of the *c*-dipole moment component, as shown in Figure 1. The potential energy curve of the proton inversion process was calculated by varying the angle $\beta = \arccos\left(\frac{\overrightarrow{C_cN} \cdot \overrightarrow{NH}}{|C_cN| \cdot |NH|}\right)$ between the plane containing the heavy atoms and the amino-hydrogen bond in steps of 2.86° within a range of 0° to 90° due to symmetry. C_c is the center between the carbon atoms C_7 and C_3. All other molecular parameters were optimized using the same three levels of theory mentioned in the preceded section. The obtained energies were parameterized and the obtained potential energy curves with a double minimum are illustrated in Figure 3. The calculated energies are presented in Table S-VI in the Supplementary Material.

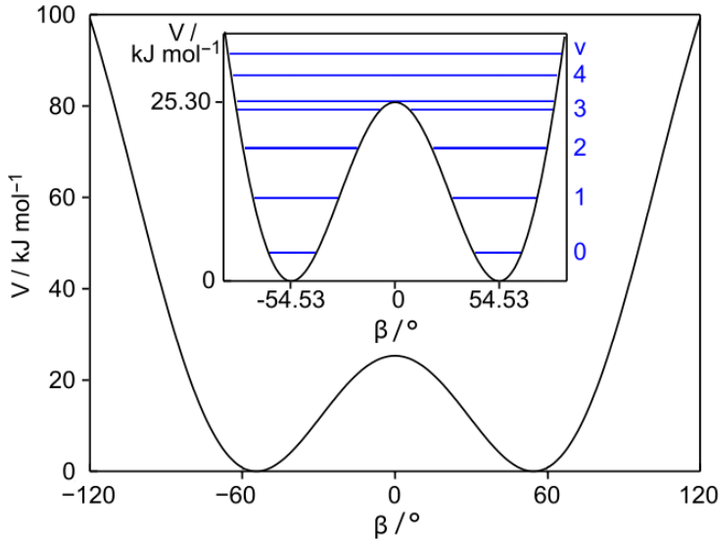

FIG. 3: The double minimum potential of the proton tunneling inversion process of conformer 1 of EMA. The angle β is defined as the angle between the NH bond and the NCC plane. The inset shows the barrier height calculated from the $v = 0$ inversion splitting and the inversion levels that split into a (+) and (–) sublevel. Calculations of the energy levels were carried out as described in the Appendix of Ref. 10.

The minima of the double-well potential curve are located at $\beta = \pm 54.53°$ and the local maximum is at $\beta = 0°$, which describes a pseudo sp^2 configuration of the nitrogen atom with the amino hydrogen and the neighboring carbon atoms being co-planar. Electron delocalization due to the lone electron pair makes this sp^2 configuration, however, a transition state. The tunneling barriers calculated with the MP2, B3LYP, and B3PW91 methods are 25.32, 18.48, and 18.52 kJ·mol^{-1}, respectively. In the regions of $\beta < -54.53°$ and $\beta > 54.53°$, the potential energy increases rapidly due to the close proximity of amino-hydrogen to the alkyl groups. Calculations outside the [–90°, 90°] range did not converge.

Due to the inversion motion of the amino proton, the vibrational ground state level splits into a lower symmetric and a higher anti-symmetric sublevel, henceforward called the (+) and the (−) state, respectively. Because the sign of the *c*-dipole moment component changes upon inversion, the selection rules (+) ↔ − and (−) ↔ (+) are obtained for *c*-type transitions. On the other hand, the sign of the *b*-dipole moment component retains during the inversion process, causing the selection rules (+) ↔ (+) and (−) ↔ (−) for *b*-type transitions. The dependency of the inversion splittings between the (+) and (−) energy levels on J and K is accounted for by the operator H_E which can be formulated as

$$\mathcal{H}_E^v = vE + \frac{1}{2}(-1)^v(E_J P^2 + E_K P_a^2 + E_2(P_+^2 + P_-^2) + E_{JK} P^2 P_a^2) \quad (4)$$

where E defines the difference between the (+) and (−) states and E_J, E_K, E_2, and E_{JK} describe perturbations of higher order. In the microwave spectrum of dimethyl amine[8] and diethyl amine,[10] the (+) and (−) states are separated by $E \approx 1323.0$ and 760.8 MHz, respectively. Consequently, all *c*-type transitions split into doublets separated by twice the value of E, which is about 2646.0 MHz for the manner and 1521.5 MHz for the latter molecule. In the previous investigation on ethyl methyl amine, Penn and Boggs also reported a tunneling splittings of about 1981.0 MHz for all *c*-type transitions.[9]

The Coriolis coupling operator $H_C = F_{ac}(P_a P_c + P_c P_a) + F_{bc}(P_b P_c + P_c P_b)$ connects the (+) and (−) energy levels. According to selection rules, *b*-type transitions are not split. However, in the microwave spectrum of diethyl amine, which was recorded using the same instrumental setup, we observed narrow splittings of about 100 kHz due to the influence of Coriolis coupling.[10] Such splittings of *b*-type transitions are also expected in the spectrum of ethyl methyl amine.

III. EXPERIMENTAL SECTION

A. Measurements

All spectra of ethyl methyl amine were measured using a MJ-FTMW spectrometer operating from 2 to 26 GHz which is a modified version of the spectrometer described in Ref. [22]. The experimental resolution of 2 kHz is more than 10 times better than that of 25 kHz of the Stark modulated spectrometer used in Ref. [9], therefore enabling us to resolve the small splittings arising from the internal rotation of both methyl groups. The substance bought from TCI Europe, Zwijndrecht, Belgium, with a purity of over 98.0% was used as received. The gas mixture for the measurement was composed of 1% EMA in Helium as inert carrier gas at a pressure of approximately 1 bar for intense signals and between 0.2 to 0.4 bar for weaker ones.

B. Spectral Assignment

First of all, predictions for the proton inversion tunneling transitions and ^{14}N-quadrupole hyperfine structure were carried out with the program *SPCAT*.[23] The rotational constants A, B, C and the tunneling constant E was taken from Ref. [9], the quadrupole coupling constants χ_{aa} and $\chi_{bb} - \chi_{cc}$ were obtained by quantum chemical calculations (see section II-B).

The spectra for the first fit included the *Q*-branch *c*-type transitions $4_{14} \leftarrow 4_{04}$, $5_{15} \leftarrow 5_{05}$, $6_{16} \leftarrow 6_{06}$ and the *Q*-branch *b*-type transitions $2_{11} \leftarrow 2_{02}$, $3_{12} \leftarrow 3_{03}$, $4_{13} \leftarrow 4_{04}$, and $5_{14} \leftarrow 5_{05}$. Each of the *c*-type transitions were split into a (−) ← (+) and a (+) ← (−) transition with a separation of about 1980 MHz, which were further split into several ^{14}N quadrupole hyperfine transitions. The number and intensity of hyperfine components vary, depending on the respective rotational transition. Each of the ^{14}N quadrupole hyperfine component appears as a quartet arising from the torsional fine structure. For a molecule with two inequivalent methyl internal rotors, each rotational transition splits into five torsional species called $(\sigma_1\sigma_2)$ = (00), (01), (10), (11), and (12).[24] The numbers σ = 0, 1, 2 represent the three symmetry species A, E_a, E_b of the C_3 group, respectively. In the case of EMA, σ_1 refers to the amino methyl and σ_2 to the ethyl methyl group. In all transitions, the separation between the (11) and (12) species are below the resolution limit of the spectrometer. Therefore, the fine structure is characteristic by a quartet instead of a quintet. Figure 4 shows a typical spectrum of the (−) ← (+) component of the *Q*-branch *c*-type transition $5_{15} \leftarrow 5_{05}$.

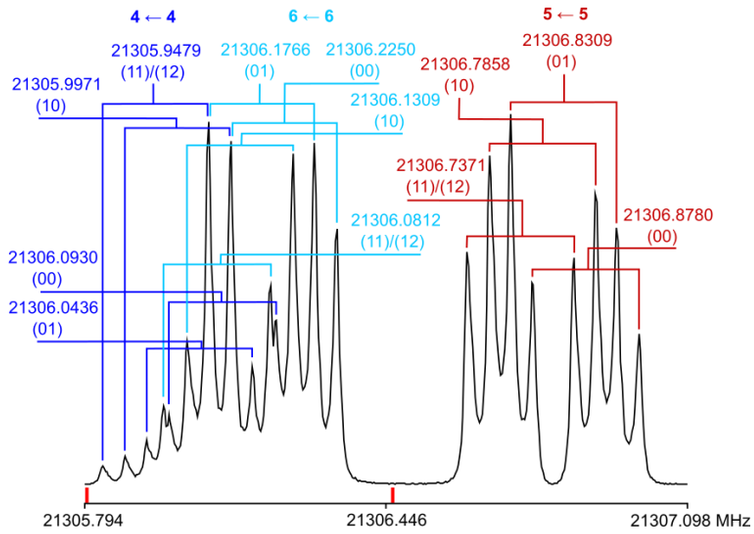

FIG. 4: The spectrum of the (−) ← (+) component of the *c*-type transition $5_{15} \leftarrow 5_{05}$. Two spectra measured at the polarization frequencies of 21305.5 MHz and 21306.5 MHz (marked in red) are combined and the intensities are normalized. All frequencies are given in MHz. The displayed frequencies are the mean values of the Doppler doublets marked by brackets. The respective torsional species are given after each frequency, and the ^{14}N quadrupole hyperfine component $F' \leftarrow F$ is above each torsional block.

The spectrum illustrated in Figure 4 shows two separate multiplets. The left hand-side multiplet contains two overlapping $F \leftarrow F$ blocks with $F = J \pm 1$ (in blue and cyan) and the right hand-side multiplet only consists of an $F \leftarrow F$ with $F = J$ component (in red). This two-block structure is typical for *c*-type transitions. Each line

appears as a doublet due to the co-axial arrangement of the molecular jet and the mirrors of the spectrometer. The splittings of these Doppler doublets and of the internal rotation quartets are essentially constant within one rotational transition and can be determined accurately with the separate $F = J \leftarrow J$ component. The (00) species always possesses the highest frequency, followed by the (01), (10), and (11)/(12) species. The separation between (00) and (01), (01) and (10), and (10) and (11)/(12) is from 30 to 50 kHz. After the torsional fine structure and the Doppler splitting had been determined from the separate $F = J \leftarrow J$ component, the assignment of the two overlapping $F = J \pm 1 \leftarrow J \pm 1$ components at lower frequencies was straightforward by assuming the same splittings for both the Doppler doublets and the torsional structure. All *Q*-branch *c*-type transitions with $J \geq 5$ feature the characteristic structure aforementioned.

For *b*-type transitions, the *F*-components of the quadrupole hyperfine pattern appear in reverse order compared to that of the *c*-type transitions, i.e. the separate $F = J \leftarrow J$ component is at lower frequency and the overlapping $F = J \pm 1 \leftarrow J \pm 1$ components are higher in frequency. The spectral assignment is more complicated, because the (+) ← (+) and the (−) ← (−) species are not degenerated due to the influence of Coriolis coupling, causing additional splittings in the same order of magnitude as those arising from the internal rotation and the Doppler effects. Figure 5 illustrates a typical spectrum of the separate $F = 3 \leftarrow 3$ component of the *b*-type $3_{12} \leftarrow 3_{03}$ transition.

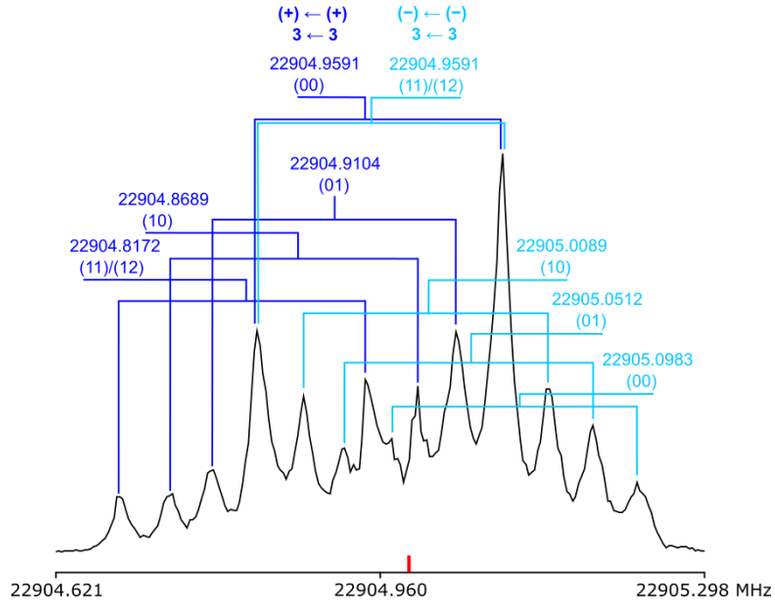

FIG. 5. The spectrum of the hyperfine component $F = 3 \leftarrow 3$ of the *b*-type $3_{12} \leftarrow 3_{03}$ transition measured at the polarization frequency of 22905.0 MHz (marked in red). All frequencies are given in MHz. The displayed frequencies are the mean values of the Doppler doublets marked by brackets. The respective torsional species are given after each frequency. The corresponding (+) ← (+) and (−) ← (−) species are color-coded and given above each torsional block.

For *Q*-branch *c*-type transitions with $J \leq 4$ and for *b*-type transitions with $J \leq 2$, some $F \leftrightarrow F + 1$ components could be measured in addition. Two *R*-branch *b*-type transitions $4_{04} \leftarrow 3_{13}$ and $5_{05} \leftarrow 4_{14}$ were also found, where the $F \leftrightarrow F + 1$ components were intense while the $F \leftrightarrow F$ components could not be measured.

IV. RESULTS AND DISCUSSION

A. The *SPFIT/SPCAT* fit

A global analysis of the overall rotation, the proton inversion tunneling, and the ^{14}N nuclear quadrupole coupling was performed using the program *SPFIT/SPCAT*[23] with a total of 142 lines. The fitted parameters are presented in Table III; the frequency lists in Table S-VII of the Supporting Information.

TABLE III. Molecular parameters of ethyl methyl amine obtained from the *SPFIT/SPCAT* code taking into account the overall rotation, proton tunneling, and ^{14}N quadrupole coupling effects.

Par.[a]	Unit	*SPFIT*	MP2[b]
A	MHz	25934.717(21)	26058.648
B	MHz	3919.8212(23)	3928.889
C	MHz	3669.530(21)	3677.933
D_J	kHz	0.8529(48)	0.8628
D_{JK}	kHz	−2.001(26)	−2.801
d_1	kHz	−0.07911(24)	−0.0779
d_2	kHz	15.8(11)	0.00005
E	MHz	990.45840(31)	
E_J	kHz	−56.72(91)	
E_K	kHz	−66.91(12)	
E_{JK}	kHz	−1.568(32)	
E_2	kHz	−25.93(45)	
F_{bc}	kHz	340.9(71)	
F_{ac}	MHz	163.9(14)	
χ_{aa}	MHz	2.78865(55)	2.77903
$\chi_{bb} - \chi_{cc}$	MHz	4.63045(91)	4.45665
σ^c	kHz	6.0	
N^d		142	

[a] All parameters refer to the principal axis system. Watson's S reduction in the I^r representation was used. Standard error in parentheses is in the units of the last digits.

[b] Equilibrium rotational constants calculated at the MP2/6-311++G(d,p) level of theory. The rotational constants of the vibrational ground state are A_0 = 25752.292 MHz, B_0 = 3888.398 MHz, and C_0 = 3640.080 MHz. Centrifugal distortion constants are obtained by anharmonic frequency calculations at the same level of theory (D_K = 53.984 kHz). NQCC values are calculated at the B3PW91/6-311+G(df,pd)//MP2/6-311++G(d,p) level.

[c] Root-mean-square deviation of the fit.

[d] Number of lines.

Due to the large value of the *A* rotational constant, only transitions with $K_a = 0, 1$ could be recorded with the spectrometer in use. Though the experimental accuracy is about 2 kHz,[25] signals of all multiplets overlap and cause line broadening that can also contain unresolved spin-spin or spin-rotation coupling splittings. In some cases, signals of hyperfine components with lower intensity overlap with those of higher intensity and appear as shoulders, whose frequencies cannot be determined with the same accuracy as those of clearly defined peaks. Furthermore, the signal-to-noise ratio of *c*-type transitions with $J \geq 11$ and *b*-type transitions with $J \geq 4$ is often low, which also influence the precision of the line frequencies. Finally, only the (00) species lines are considered in the *SPFIT* fit and the internal rotation effects have been neglected. Therefore, the root-mean-square deviation of 6.0 kHz is satisfactory. The molecular parameters are determined with much higher accuracy compared to the previous work of Penn and Boggs.[9]

The values of the experimental deduced rotational constants A = 25934.717(21) MHz, B = 3919.8212(23) MHz, and C = 3669.530(21) MHz are close to those predicted at the MP2/6-311++G(d,p), B3LYP/6-311++G(d,p), and B3PW91/6- 311++G(d,p) levels of theory. Centrifugal distortion constants obtained by anharmonic frequency calculations at the MP2/6-311++G(d,p) level of theory mostly show results close to the experimental values except for d_2. The E parameter describing the splittings of *c*-type transitions due to proton tunneling is 990.45884(31) MHz, which is significantly more precise than the value of 990.20 MHz reported in Ref. [9]. The higher order parameters E_J, E_K, E_{JK}, and E_2 as well as the Coriolis coupling terms F_{bc} and F_{ac} are well-determined. The ^{14}N NQCCs deduced from the *SPFIT/SPCAT* fit are accurate and match the values calculated at the B3PW91/6-311+G(df,pd)//MP2/6-311++G(d,p) level.

B. The *XIAM* fit

To determine the barrier to internal rotation, the torsional fine splittings were fitted with the program *XIAM*.[26] The values for the angles between the internal rotor axes and the principal axes of inertia were taken from *ab initio* geometry and kept fixed. All other parameter values such as the rotational constants and the nuclear quadrupole constants, were also fixed to the values of the *SPFIT/SPCAT* fit, and only the V_3 potentials were floated. As *XIAM* cannot consider the tunneling effects, the torsional splittings $\nu_{(01)} - \nu_{(00)}$, $\nu_{(10)} - \nu_{(00)}$, and $\nu_{(11)/(12)} - \nu_{(00)}$ were fitted instead of the absolute line frequencies. The barriers to internal rotations were found to be 1048.62(41) and 1163.43(80) cm^{-1} for the amino methyl and the ethyl methyl group, respectively, which are in good agreement with the calculated values. Surprisingly, the barrier height of the amino methyl group of EMA is closer to the value of 1051.74(57) cm^{-1} found for the ethyl methyl group in diethyl amine[10] and some other methyl groups at the end of an alkyl chain[19-21] while the barrier height of the ethyl methyl group of EMA is significantly higher, but close

to the values observed for the ethyl methyl torsion of many other molecules e.g. ethyl acetate (1112.3(37) cm^{-1})[27] and ethyl fluoride (1171.3(14) cm^{-1}).[28] The result of the *XIAM* fit is given in Table IV. The frequency list is available in Table S-VII of the Supplementary Material.

TABLE IV. Experimental barrier heights to internal rotation for the amino methyl i_M group ($V_{3,M}$) and the ethyl methyl i_E group ($V_{3,E}$) determined with the *XIAM* code and values calculated at the MP2/6-311++G(d,p) level of theory.

Par.[a]	Unit	Value
$V_{3,M}$	cm^{-1}	1084.62(41)
$V_{3,M}$	cm^{-1}	1105.10[b]
$V_{3,E}$	cm^{-1}	1163.43(80)
$V_{3,E}$	cm^{-1}	1178.84[b]
I_α	$uÅ^2$	3.159[b]
$\angle(i_M,a)$	deg	154.236[b]
$\angle(i_M,b)$	deg	88.388[b]
$\angle(i_M,c)$	deg	64.294[b]
$\angle(i_E,a)$	deg	23.511[b]
$\angle(i_E,b)$	deg	92.860[b]
$\angle(i_E,c)$	deg	113.316[b]
N[c]		573
σ[d]	kHz	4.6

[a] All parameters refer to the principal axis system. Watson's S reduction in I^r representation was used. Standard error in parentheses is in the units of the last digits.

[b] Values calculated at the MP2/6-311++G(d,p) level.

[c] Number of lines.

[d] Root-mean-square deviation of the fit.

V. CONCLUSION

Quantum chemical calculations were carried out at three different levels of theory, MP2/6-311++G(d,p), B3LYP/6-311++G(d,p) and B3PW91/6-311++G(d,p), yielding in total three conformers of ethyl methyl amine. Only the energetically most favorable conformer I was observed in the spectrum**.** The change in sign of the dipole moment component $|\mu_c|$ causes the selection rules (+) ← (−) and (−) ← (+) and gives rise to tunneling splittings for the *c*-type spectrum. Splittings due to proton tunneling, ^{14}N nuclear quadrupole coupling, and Coriolis coupling effects were analyzed with the program *SPFIT/SPCAT* with a total amount of 142 lines. The parameters could be determined with much higher accuracy than from the previous work of Penn and Boggs,[9] yielding accurate values for the rotation constants, quadrupole coupling constants, and the tunneling constant E = 990.45840(31) MHz.

Internal rotations arising from the two inequivalent methyl groups and the resulting fine splittings were considered with the *XIAM* code in a relative fit, resulting in barrier heights of 1084.62(41) cm^{-1} and 1163.43(80) cm^{-1} for the amino methyl and the ethyl methyl group, respectively.

SUPPLEMENTARY MATERIAL

See supplementary material for the Cartesian coordinates, potential energy curves, Fourier coefficients, and frequency lists.

DATA AVAILABLITY STATEMENT

The data that supports the findings of this study are available within the article and its supplementary material.

ACKNOWLEDGMENTS

We thank Elena Heß for her contribution within a bachelor thesis at the RWTH Aachen University. Simulations were performed with computing resources granted by the RWTH Aachen University under the project rwth0457. This work was supported by the Agence Nationale de la Recherche ANR (project ID ANR-18-CE29-0011).

REFERENCES

[1] A. Weber, Academic Press, Inc., **1st edition**, 2 (1992).

[2] M. Riese, F. Ploeger, A. Rap, B. Vogel, P. Konopka, M. Dameris, and P. Forster, J. Geophys. **117**, D16305 (2012).

[3] T. Blumestock, Atmos. Chem. Phys. **6**, 897 (2006).

[4] D. O. Muhleman and R. T. Clancy, Appl. Opt. **34**, 6067 (1995).

[5] B. Tercero, I. Kleiner, J. Cernicharo, H. V. L. Nguyen, A. López, G. M. Muñoz Caro, Astrophys. J. Lett., **770**, L13 (2013).

[6] C. P. Endres, S. Schlemmer, P. Schilke, J. Stutzki, and H. S. P. Müller, The Cologne Database for Molecular Spectroscopy, CDMS, in the Virtual Atomic and Molecular Data Centre, VAMDC. J. Mol. Spectrosc. **327**, 95 (2016). – See also the Cologne Database for Molecular Spectroscopy (CDMS) website, https://cdms.astro.uni-koeln.de/.

[7] I. Kleiner, ACS Earth Space Chem. **3**, 1812 (2019).

[8] J. E. Wollrab, V. W. Laurie, J. Chem. Phys. **48**, 5058 (1968).

[9] R. E. Penn and J. E. Boggs, J. Mol. Spectrsoc. **47**, 340 (1973).

[10] H. V. L. Nguyen and W. Stahl, J. Chem. Phy. **135**, 024310 (2011).

[11] M. J. Frisch, G.W. Trucks, H. B. Schlegel, G. E. Scuseria, M. A. Robb, J. R. Cheeseman, G. Scalmani, V. Barone, B. Mennucci, G. A. Petersson, H. Nakatsuji, M. Caricato, X. Li, H. P. Hratchian, A. F. Izmaylov, J. Bloino, G. Zheng, J. L. Sonnenberg, M. Hada, M. Ehara, K. Toyota, R. Fukuda, J. Hasegawa, M. Ishida, T. Nakajima, Y. Honda, O. Kitao, H. Nakai, T. Vreven, J. A. Montgomery, Jr., J. E. Peralta, F. Ogliaro, M. Bearpark, J. J. Heyd, E. Brothers, K. N. Kudin, V. N. Staroverov, R. Kobayashi, J. Normand, K. Raghavachari, A. Rendell, J. C. Burant, S. S. Iyengar, J. Tomasi, M. Cossi, N. Rega, J. M. Millam, M. Klene, J. E. Knox, J. B. Cross, V. Bakken, C. Adamo, J. Jaramillo, R. Gomperts, R. E. Stratmann, O. Yazyev, A. J. Austin, R. Cammi, C. Pomelli, J. W. Ochterski, R. L. Martin, K. Morokuma, V. G. Zakrzewski, G. A. Voth, P. Salvador, J. J. Dannenberg, S. Dapprich, A. D. Daniels, O. Farkas, J. B. Foresman, J. V. Ortiz, J. Cioslowski, and D. J. Fox, Gaussian, Inc., Wallingford CT (2009).

[12] B. S. Ray, Z. Phys. **78**, 74 (1932).

[13] W. C. Bailey, Chem. Phys. **252**, 57 (2000).

[14] W. C. Bailey, Calculation of Nuclear Quadrupole Coupling Constants in Gaseous State Molecules. <http://nqcc.wcbailey.net/index.html>.

[15] R. Kannengießer, W. Stahl, H. V. L. Nguyen, and W. C. Bailey, J. Mol. Spectrosc. **317**, 50 (2015).

[16] H.V.L. Nguyen and W. Stahl, ChemPhysChem. **12**, 1900 (2011).

[17] H.V.L. Nguyen, W. Stahl, and I. Kleiner, Mol. Phys. **110**, 2035 (2012).

[18] C. Dindic, W. Stahl, and H.V.L. Nguyen, Phys. Chem. Chem. Phys. (2020) accepted.

[19] M. Andresen, I. Kleiner, M. Schwell, W. Stahl, and H.V.L. Nguyen, J. Phys. Chem. A **122**, 7071 (2018).

[20] M. Andresen, I. Kleiner, M. Schwell, W. Stahl, and H.V.L. Nguyen, ChemPhysChem. **20**, 2063 (2019).

[21] M. Andresen, I. Kleiner, M. Schwell, W. Stahl, and H.V.L. Nguyen, J. Phys. Chem. A **123**, 1353 (2020).

[22] J. -U. Grabow, W. Stahl, and H. Dreizler, Rev. Sci. Instrum. **67**, 4072 (1996).

[23] H. M. Pickett, J. Mol. Spectrosc. **148**, 371 (1991).

[24] L. Ferres, J. Cheung, W. Stahl, and H. V. L. Nguyen, J. Phys. Chem. **123**, 3497 (2019).

[25] J. -U. Grabow and W. Stahl, Z. Naturforsch. **45a**, 1043 (1990).

[26] H. Hartwig and H. Dreizler, Z. Naturforsch. **51a**, 923 (1996).

[27] D. Jelisavac, D. C. Cortés-Gómez, H. V. L. Nguyen, L. W. Sutikdja, W. Stahl, and I. Kleiner, J. Mol. Spectrosc. **257**, 111 (2009).

[28] E. Fliege, H. Dreizler, J. Demaison, D. Boucher, J. Burie, and A. Dubrulle, J. Chem. Phys. **78**, 3541 (1983).

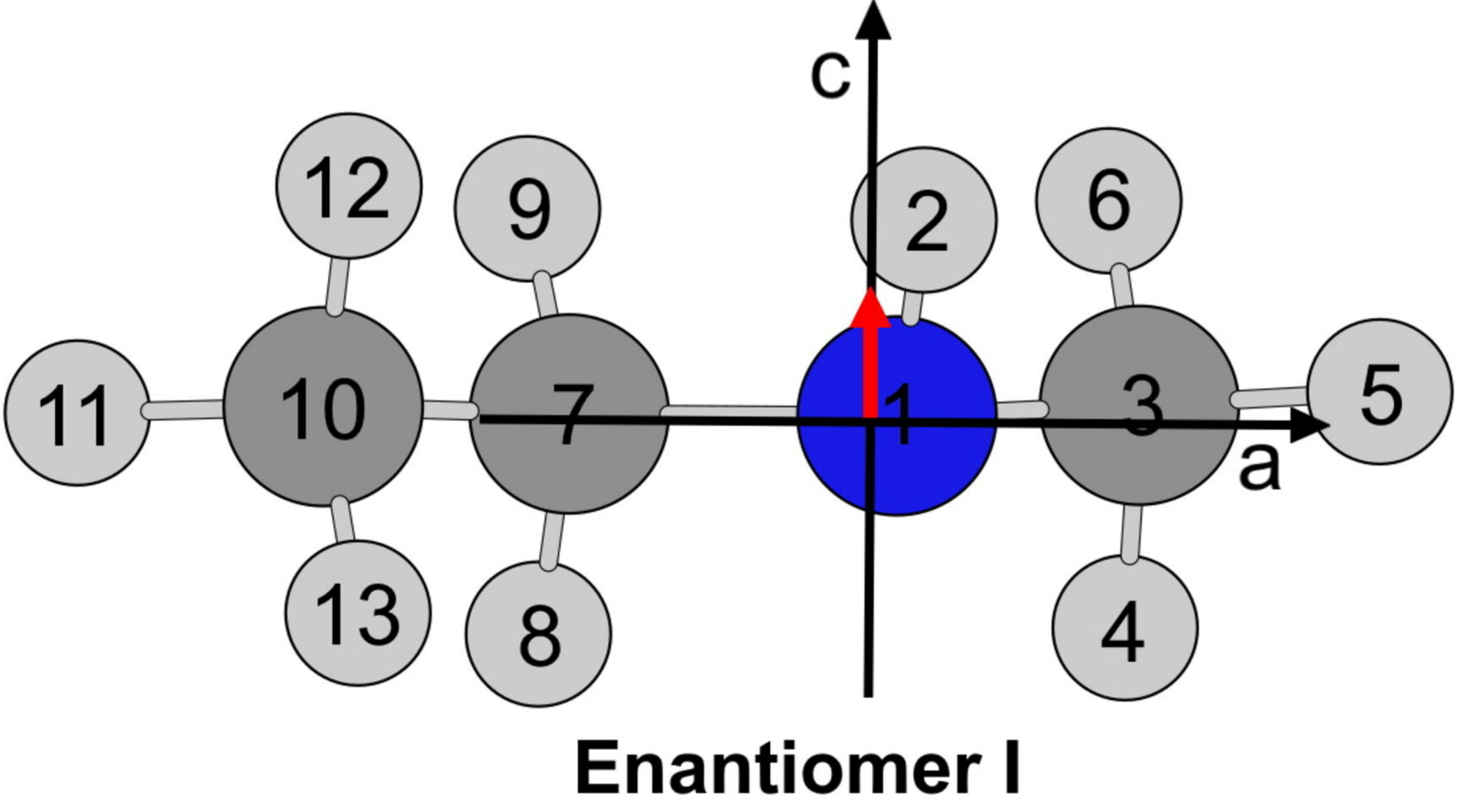

Enantiomer I

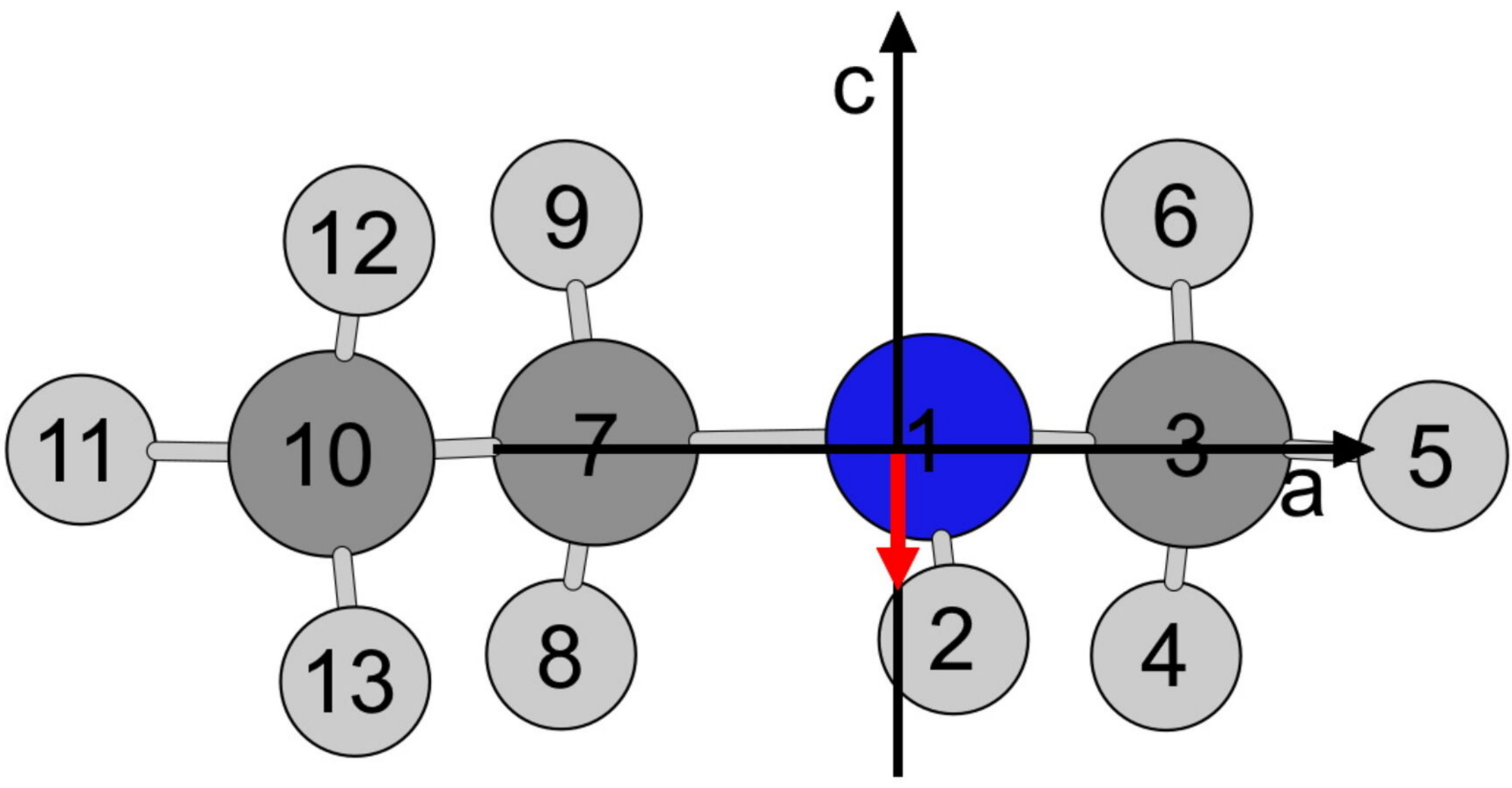

Enantiomer II

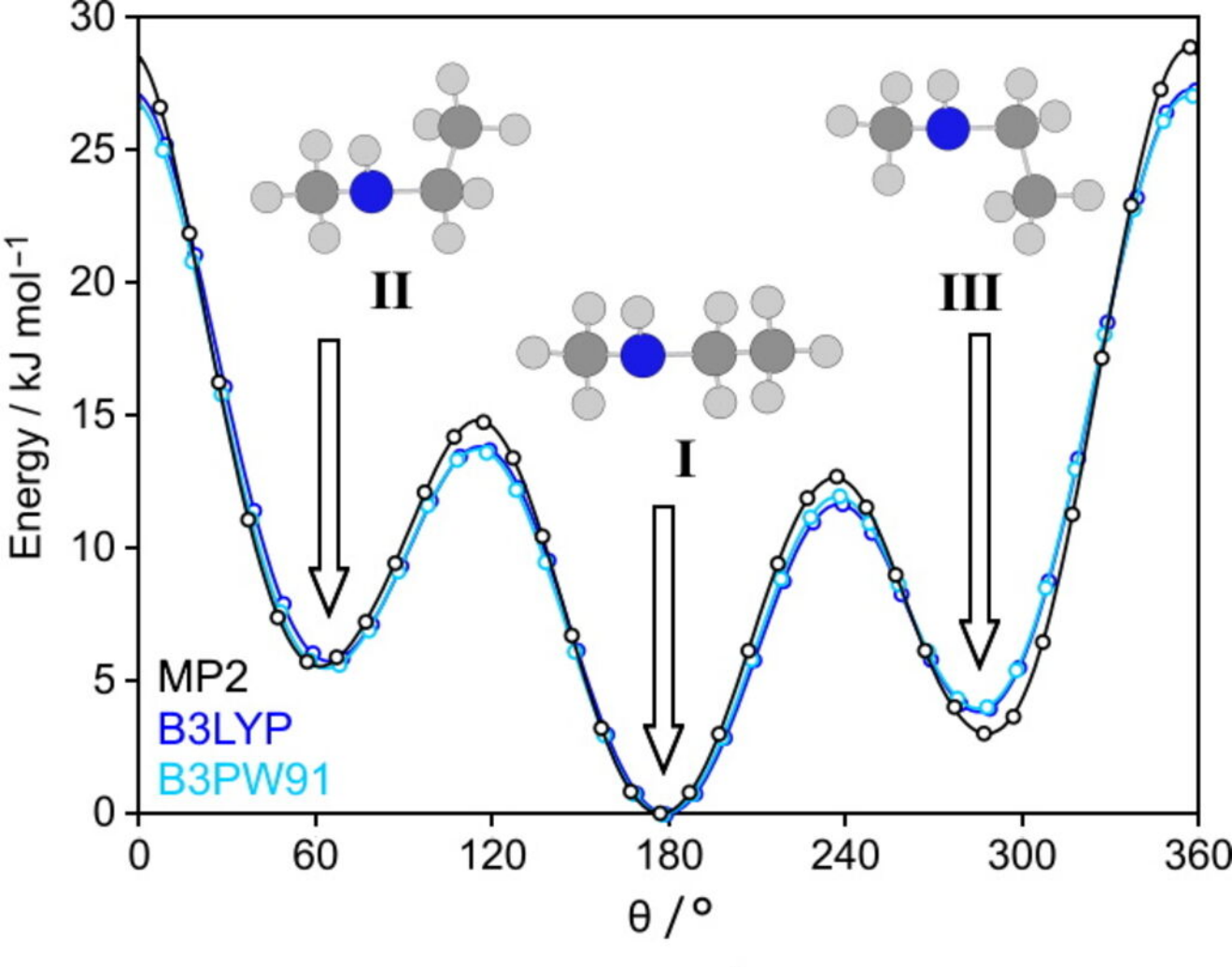

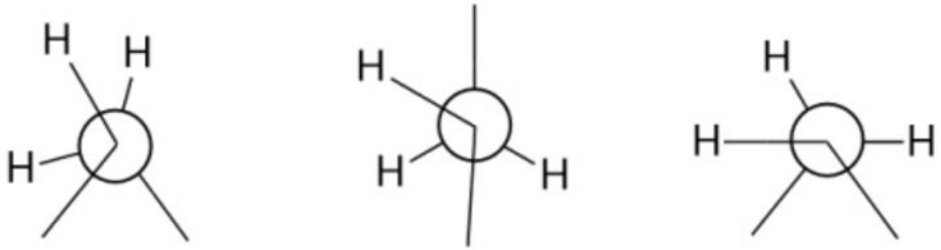

	Conformer II	Conformer I	Conformer III
MP2	-71.25°	177.01°	60.72°
B3LYP	-75.37°	178.57°	64.80°
B3PW91	-74.71°	178.40°	64.42°

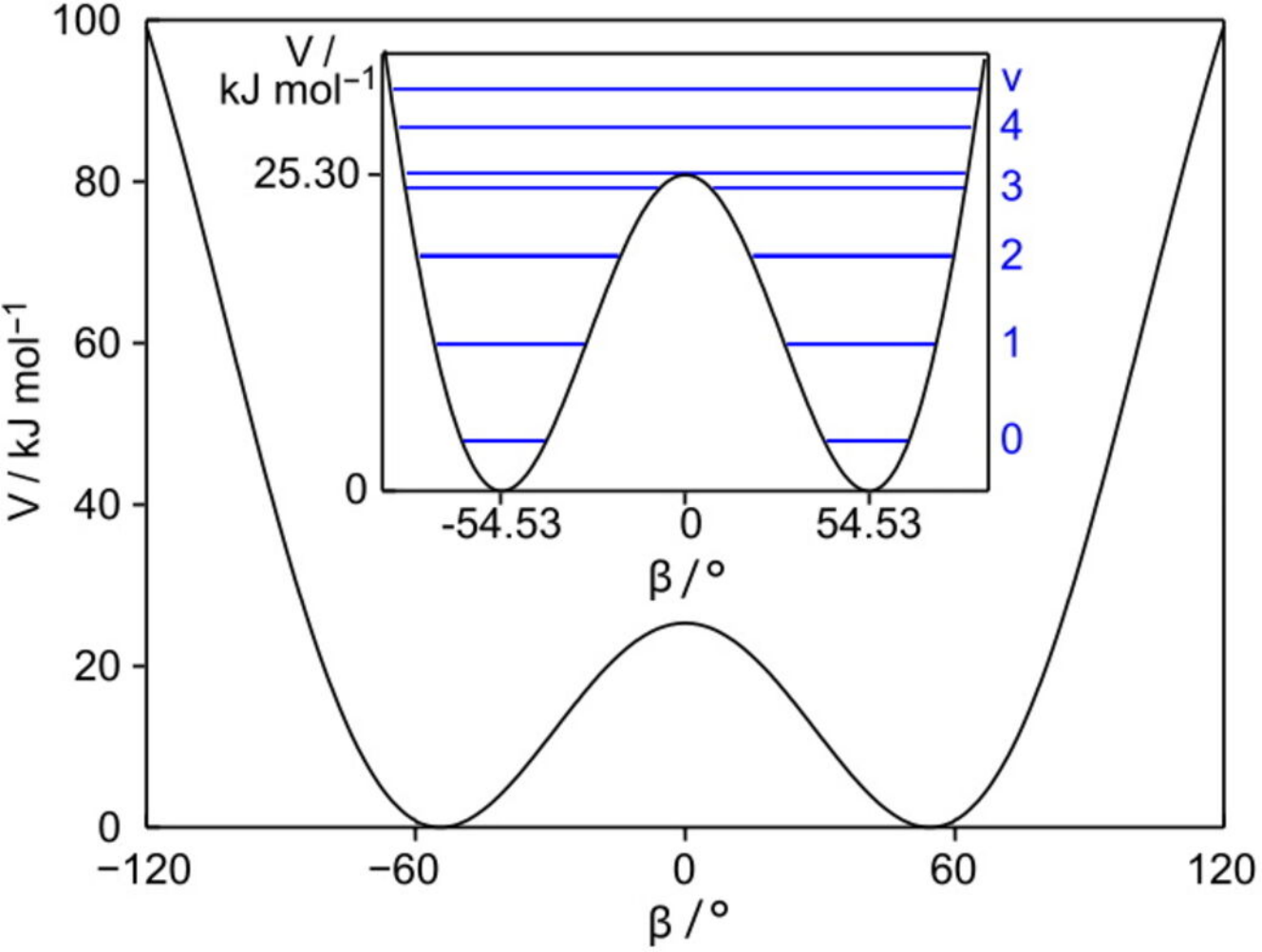
V / kJ mol⁻¹
100
80
60
40
20
0
−120
−60
0
60
120
β / °
V / kJ mol⁻¹
25.30
0
v
4
3
2
1
0
-54.53
0
54.53
β / °

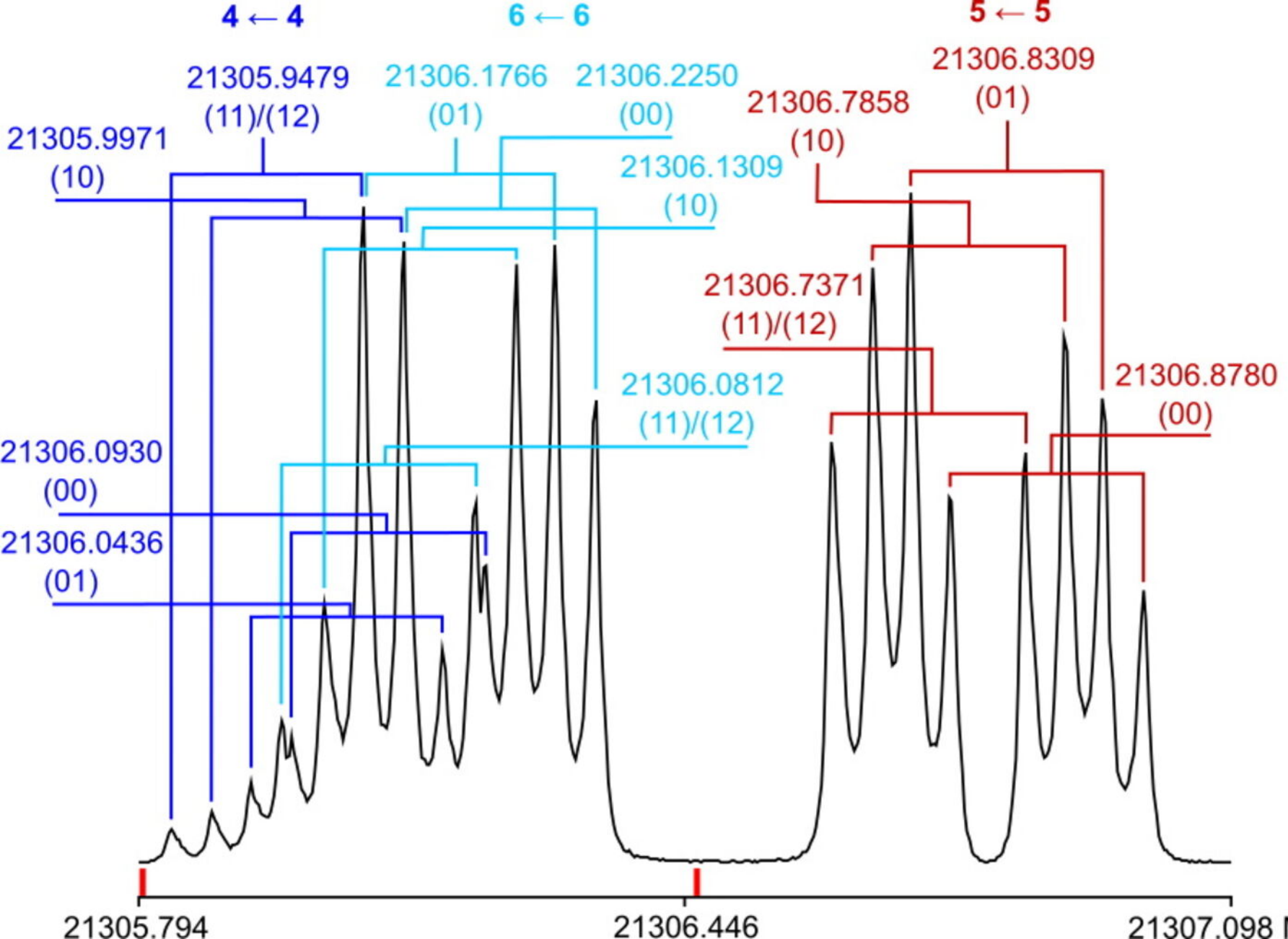
4 ← 4
6 ← 6
5 ← 5
21305.9479
(11)/(12)
21306.1766
(01)
21306.2250
(00)
21306.8309
(01)
21306.7858
(10)
21305.9971
(10)
21306.1309
(10)
21306.7371
(11)/(12)
21306.8780
(00)
21306.0812
(11)/(12)
21306.0930
(00)
21306.0436
(01)
21305.794
21306.446
21307.098 MHz

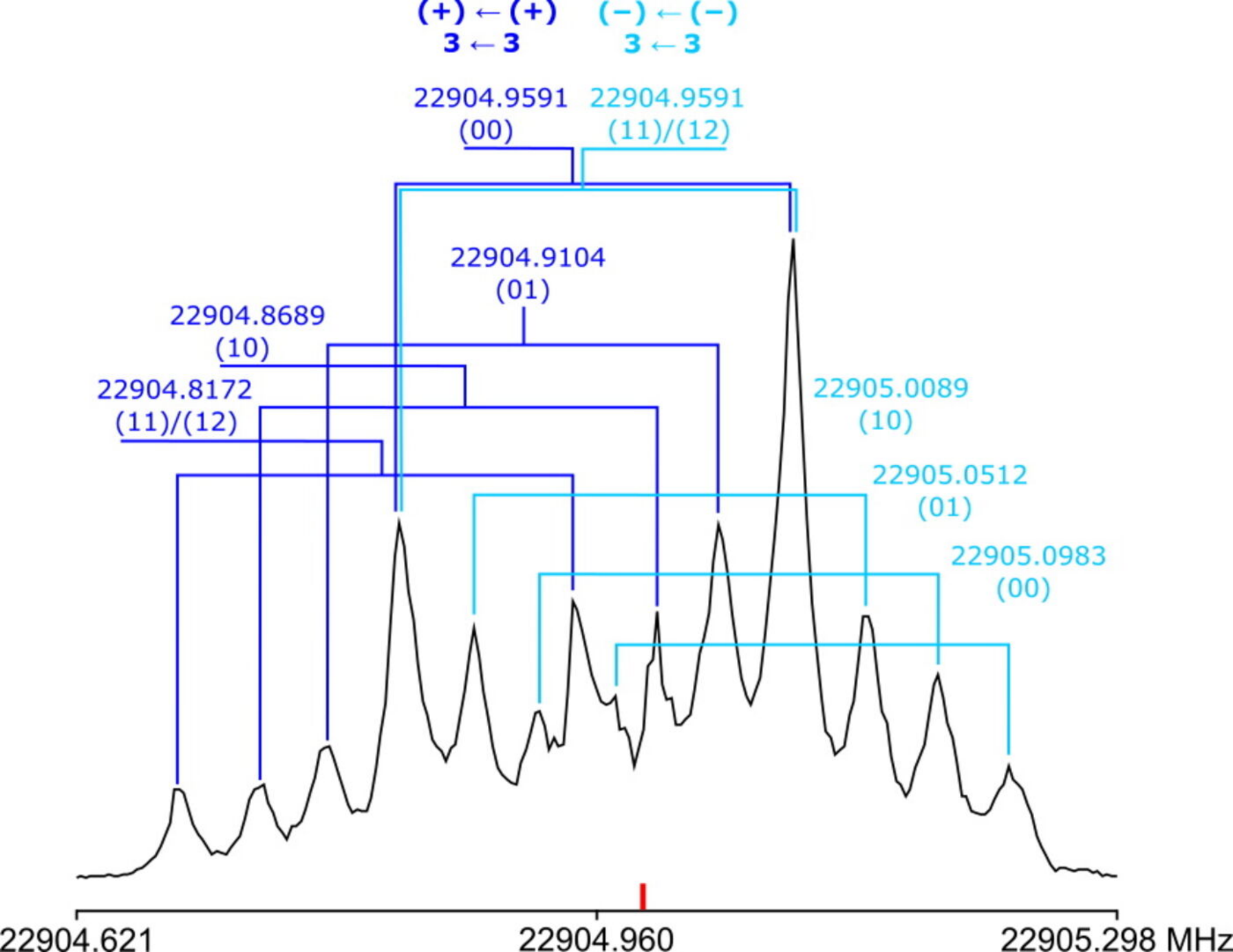
(+) ← (+)
3 ← 3
(−) ← (−)
3 ← 3
22904.9591
(00)
22904.9591
(11)/(12)
22904.9104
(01)
22904.8689
(10)
22904.8172
(11)/(12)
22905.0089
(10)
22905.0512
(01)
22905.0983
(00)
22904.621
22904.960
22905.298 MHz